**ISCI, Volume *9***

## Supplemental Information

# Immunogenomic Landscape Contributes to Hyperprogressive Disease after Anti-PD-1 Immunotherapy for Cancer

**Donghai Xiong, Yian Wang, Arun K. Singavi, Alexander C. Mackinnon, Ben George, and Ming You**

## Supplemental Information

A

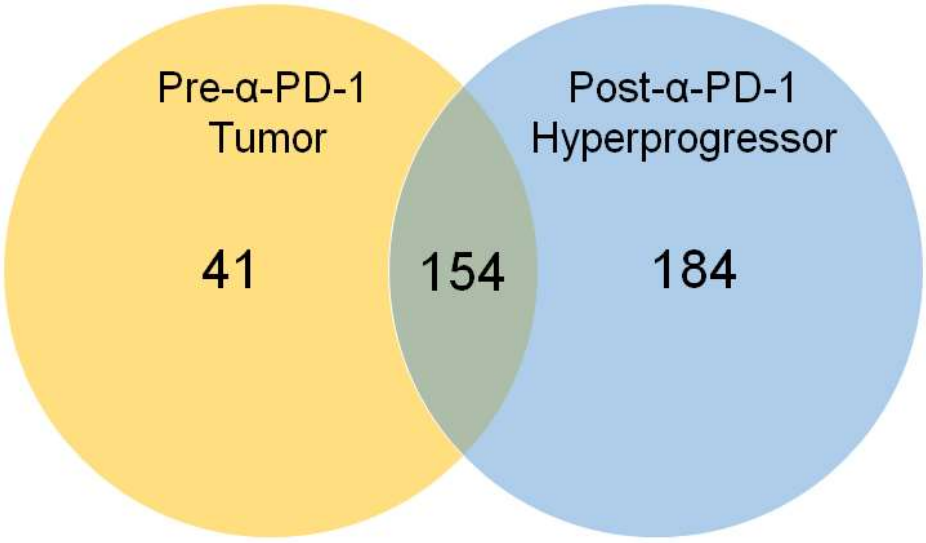


B

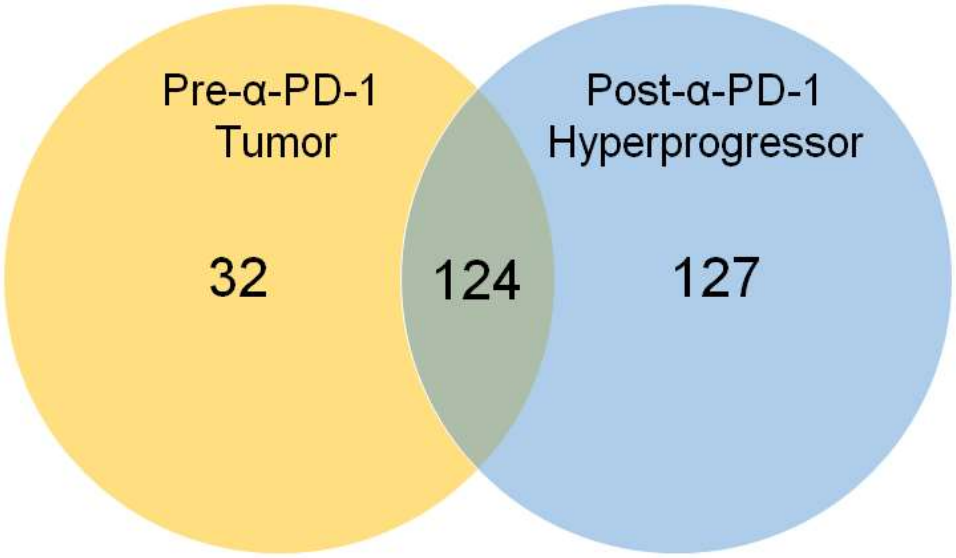


**Figure S1. The number of somatic mutations in the pre- and post- anti-PD-1 treatment tumor samples of the two patients. Related to Figure 1 and Figure 2.** A) Patient 1; B) Patient 2.

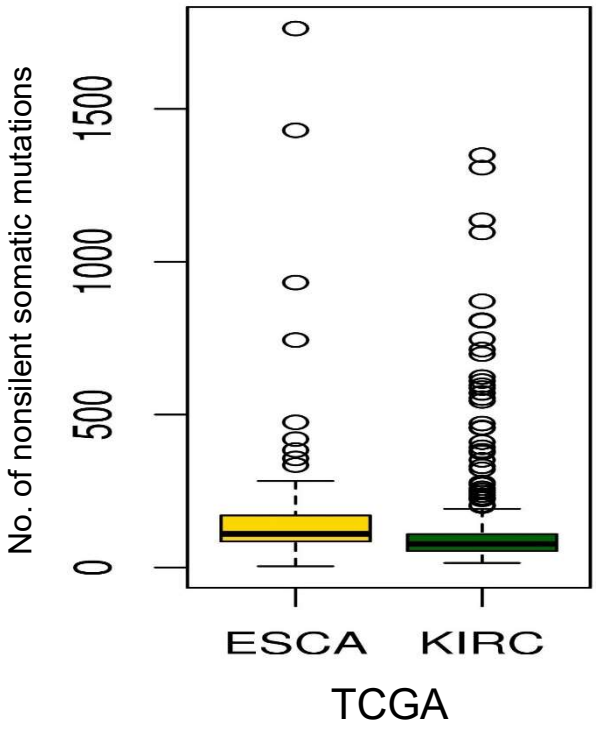


**Figure S2. The distribution of nonsilent somatic mutations in the two TCGA cancer types anaylzed in the hyperprogressive tumor context in the present study. Related to Figure 1 and Figure 2.**The numbers of nonsilent somatic mutations of the esophageal carcinoma (ESCA, n=184) and kidney renal clear cell carcinoma (KIRC, n=384) samples from TCGA.

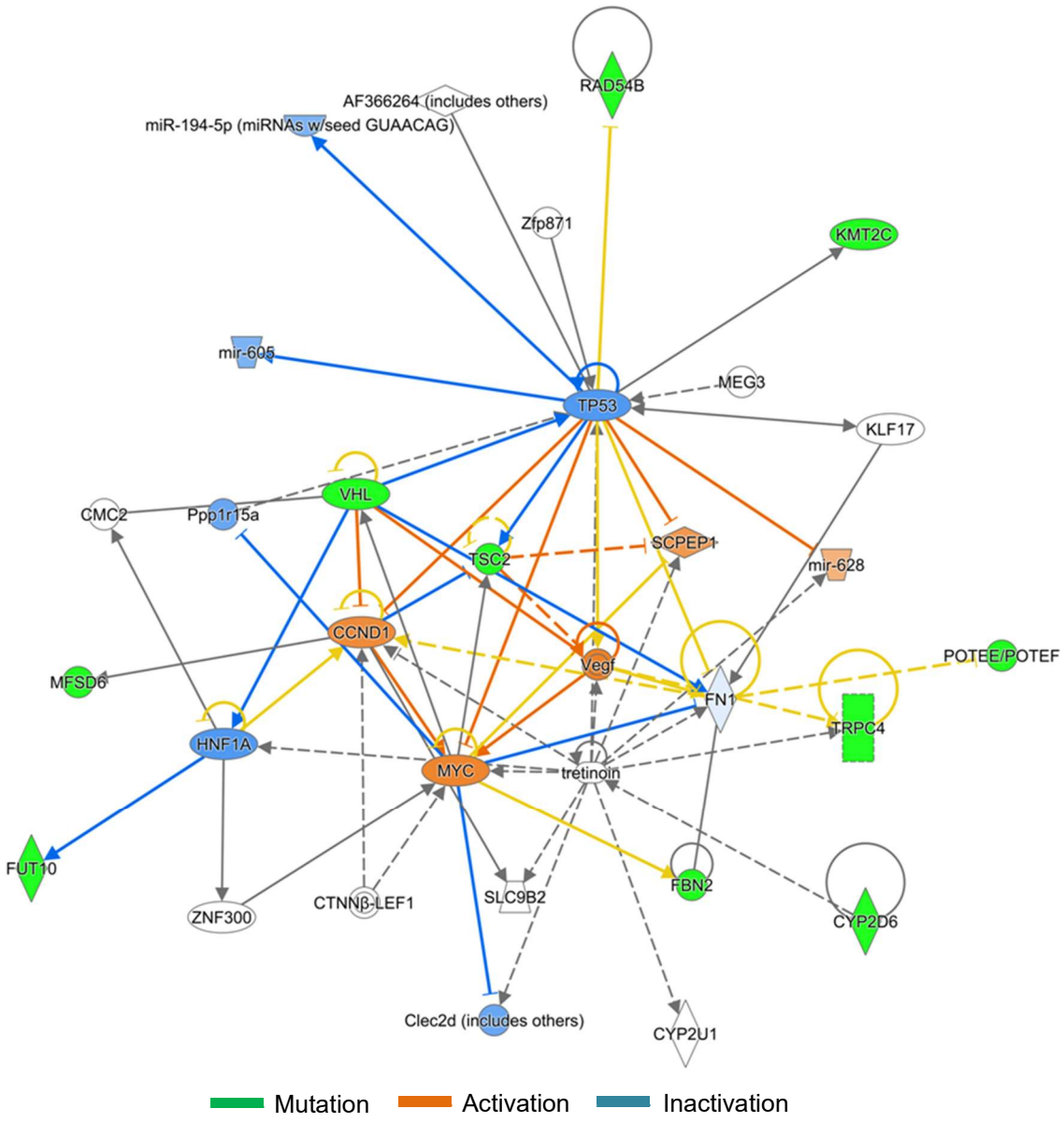


**Figure S3. Key mutated cancer genes interacting network. Related to Table 2.** Based on the eleven genes with the deleterious somatic mutations, a mechanistic network was built by IPA in which ten genes carrying these mutations resulted in the suppression of TP53 tumor suppressor pathway and activation of MYC, CCND1 and VEGF oncogenic pathways.

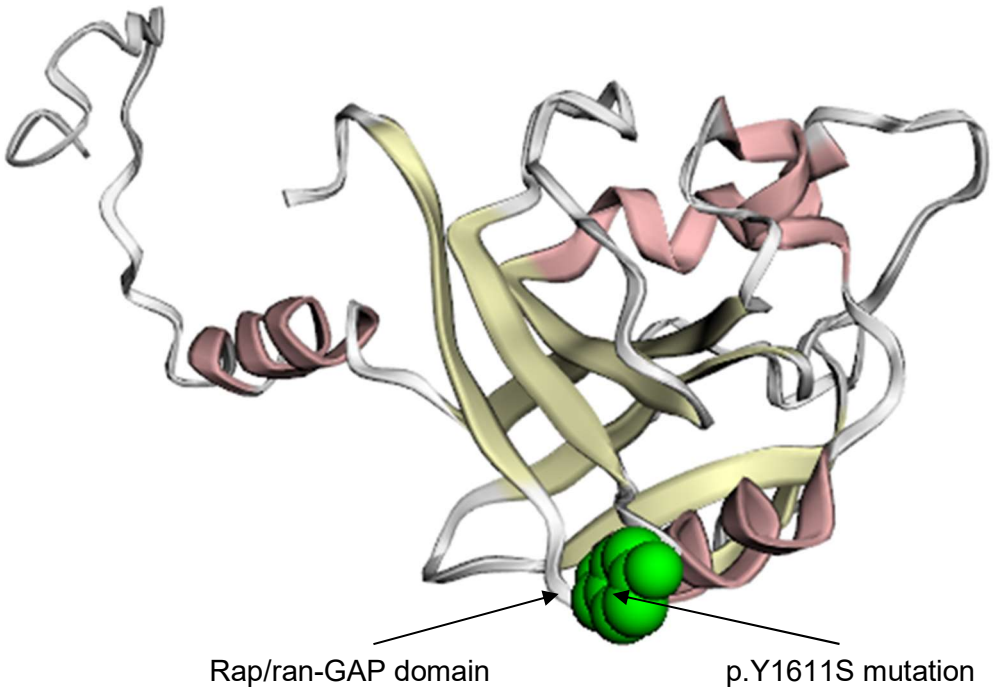


**Figure S4. Key mutation in the TSC2 protein. Related to Table 2.** The 3D structure of the TSC2 protein and the location of the amino acid residue harboring the p.Y1611S mutation, which is within the Rap/ran-GAP domain of the TSC2 protein critical to its biological function.

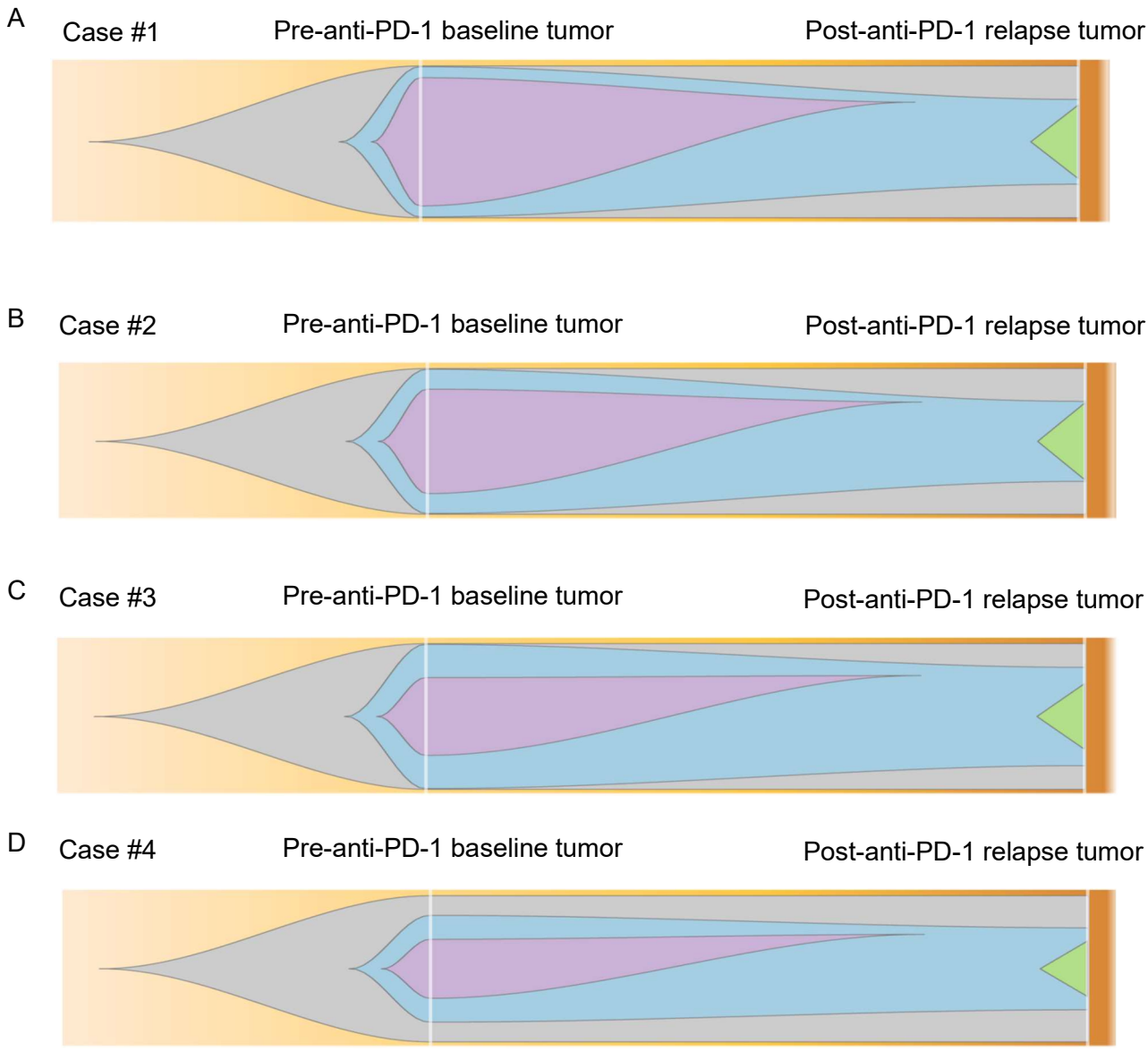


**Figure S5. Clonal evolution from the pre-anti-PD1 therapy baseline tumor to post-anti-PD-1 relapsing tumor in the four melanoma patients from a previous study. Related to Figure 4.** The graphical representation of clonal evolution in the four melanoma patients: (A) Case #1; (B) Case #2; (C) Case #3; (D) Case #4.

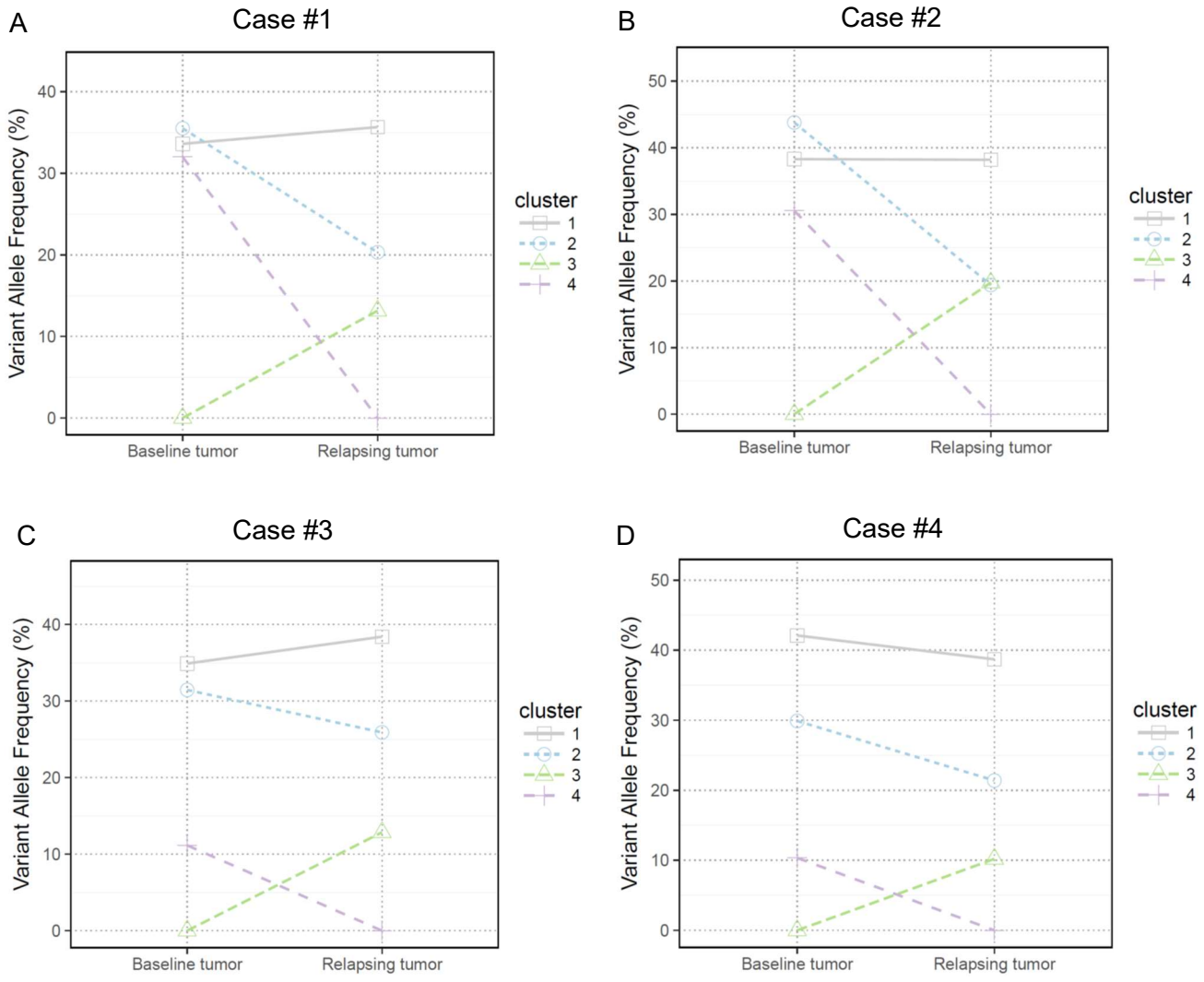


**Figure S6. The mutation clusters representing clonal evolution from the pre-anti-PD1 therapy baseline tumor to post-anti-PD-1 relapsing tumor in the four melanoma patients from a previous study. Related to Figure 4.** The mutation clusters detected in the pre-anti-PD1 therapy baseline tumor to post-anti-PD-1 relapsing tumor in the patients: (A) Case #1; (B) Case #2; (C) Case #3; (D) Case #4. The relationship between the clusters in the pre-therapy and post-therapy tumors are indicated by lines linking them.

A. ILC1 population

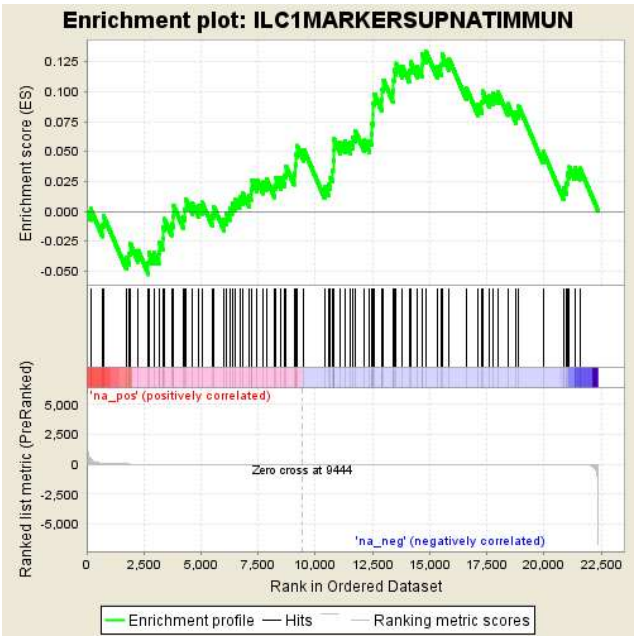


B. ILC2 population

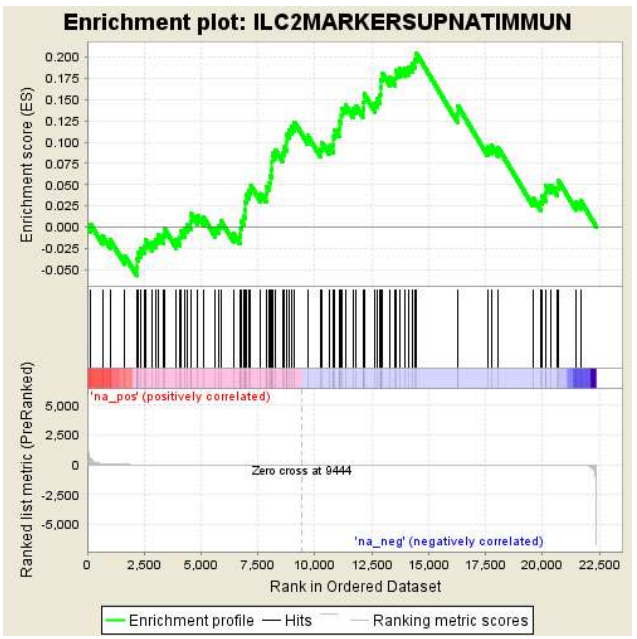


**Figure S7. The ILC1 and ILC2 populations activity do not have significant changes in the HPD tumors after anti-PD-1 therapy. Related to Figure 7.** (A) The ILC1 and (B) the ILC2 marker genes were not enriched in either the top up- or down-regulated genes in the HPD tumors.

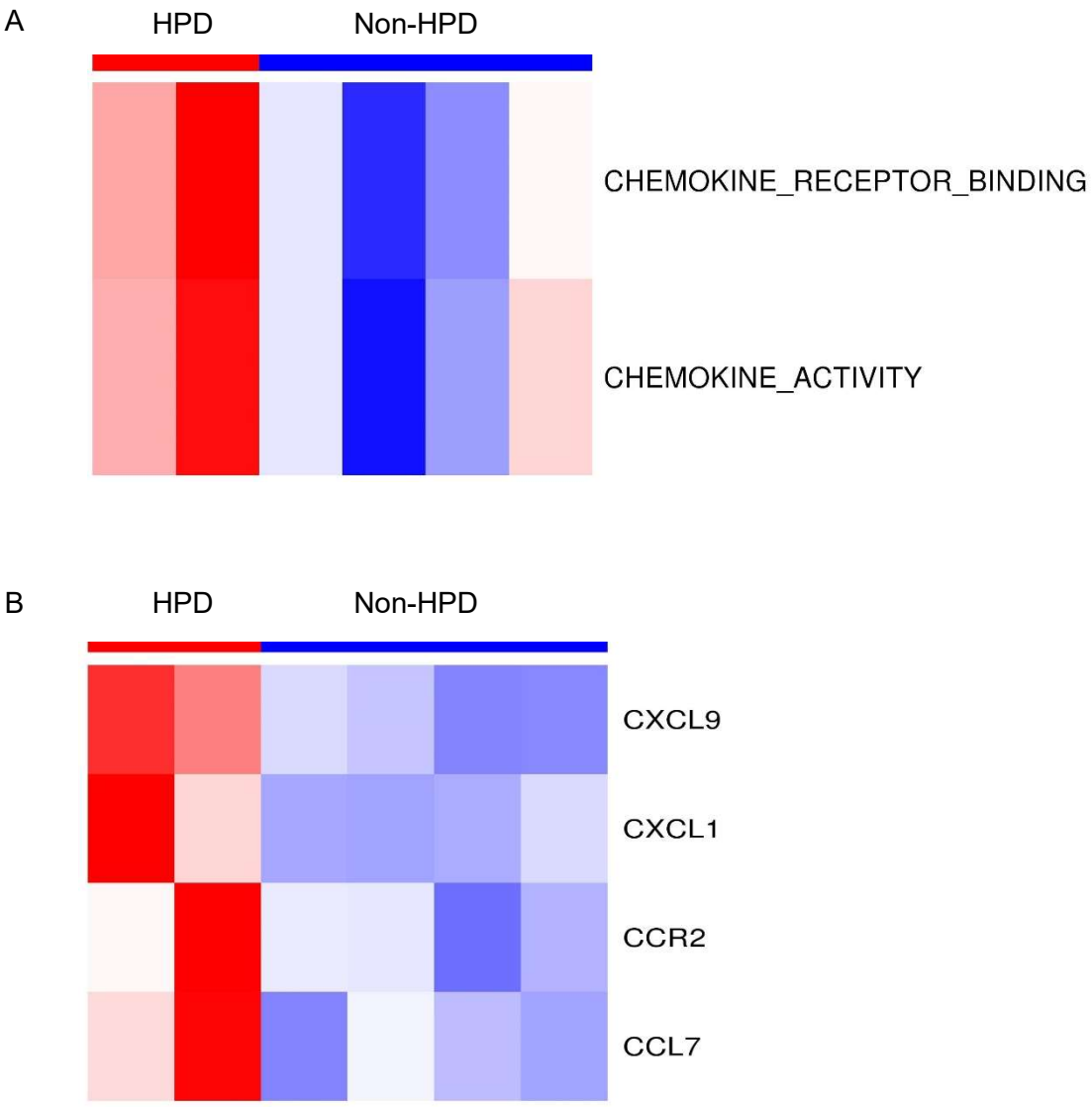


**Figure S8. Pre-α-PD-1 therapy tumors of hyperprogressive patients have elevated inflammation pathway activity (mainly chemokine activity) compared to the responsive patients. Related to Figure 8.** (A) GSVA identified the activation of two founder data sets of inflammation pathways in the pre-therapy tumors of HPD patients compared to the non-HPD patients; (B) The chemokine encoding genes that were up-regulated in the pre-therapy tumors of HPD patients compared to the non-HPD patients.

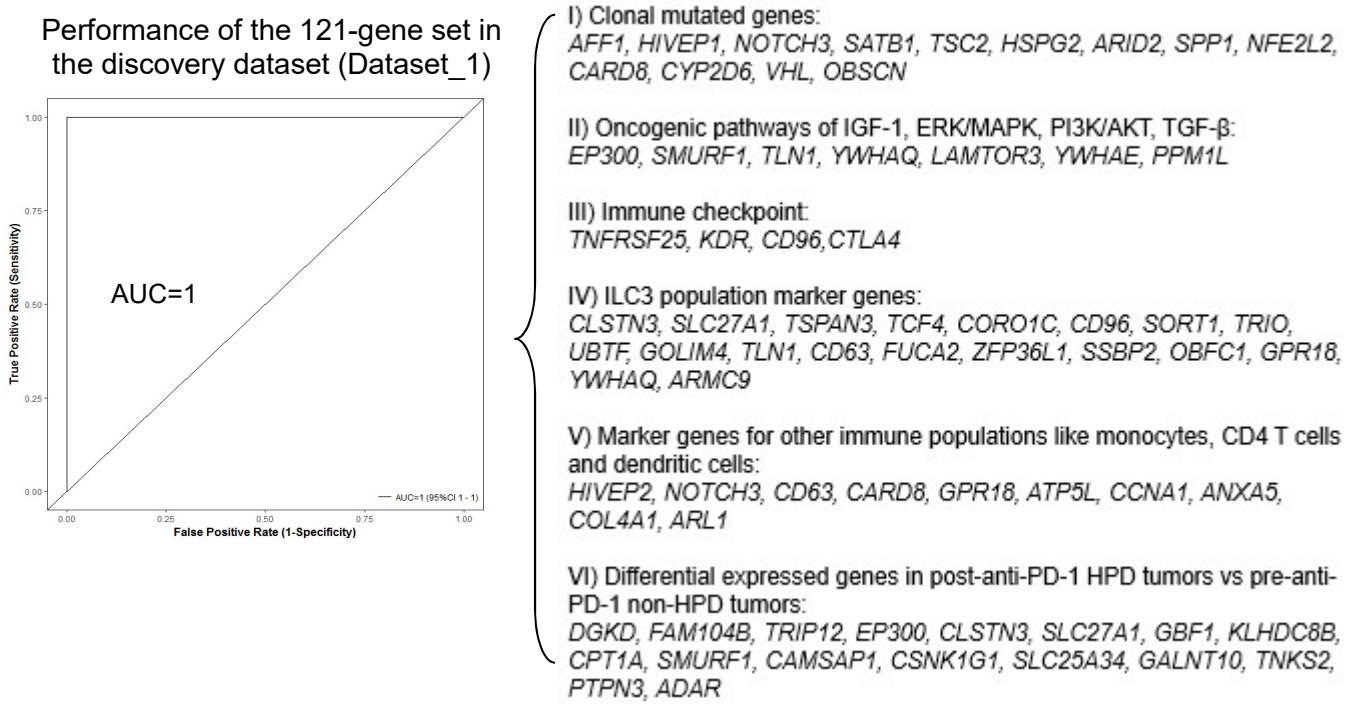


**Figure S9. Results of the 121-gene expression signature in the discovery data set (Dataset_1). Related to Figure 9.** ROC curves was shown for separating HPD patients from non-HPD patients in the discovery data set (4 HPD vs 16 non-HPD patients, AUC=1). The majority of these genes (70 of 121) belonged to the gene sets that we identified as significant to different aspects of the HPD tumors in our samples. Specifically, these genes were classified into the following six categories.

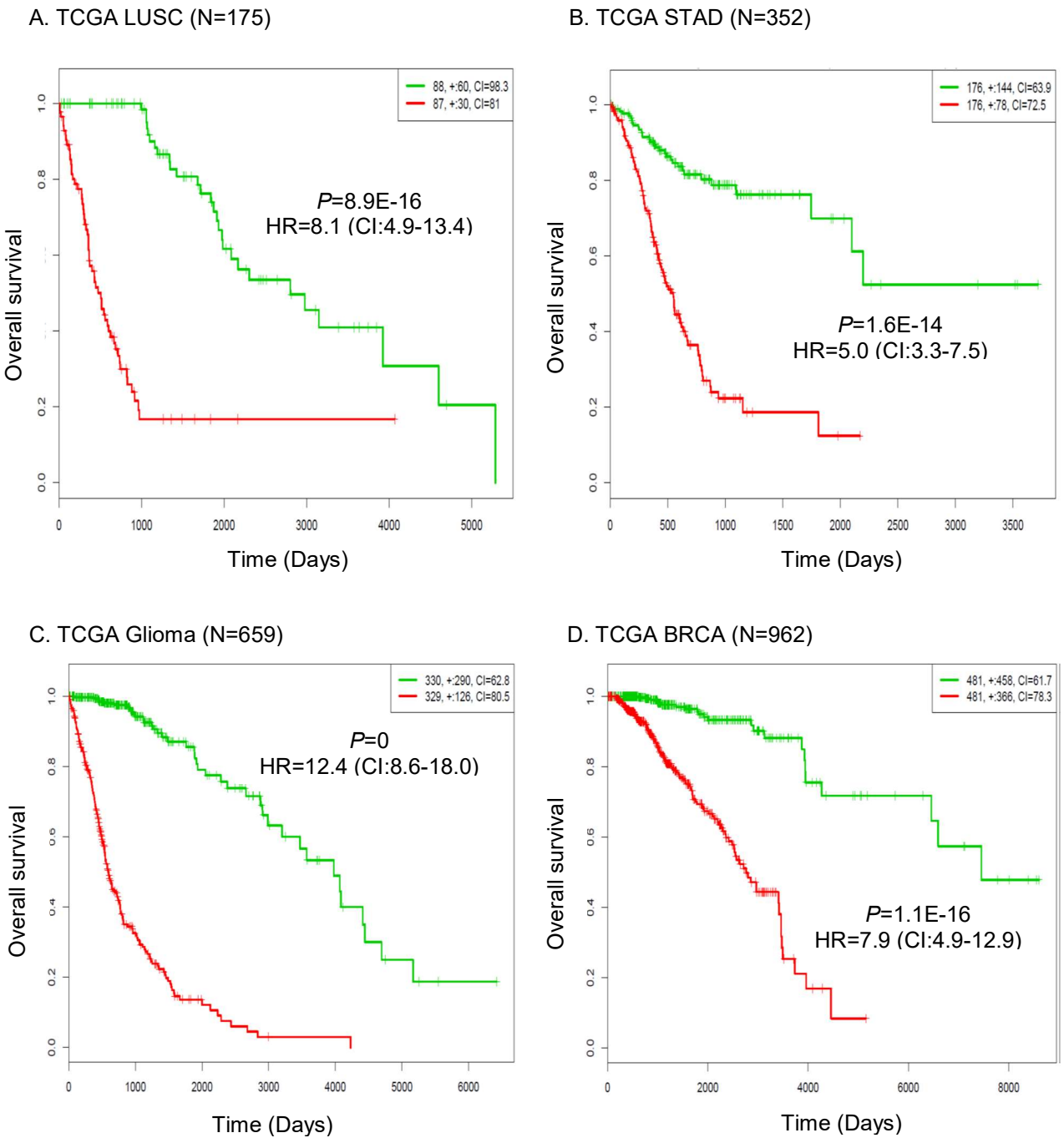


**Figure S10. Kaplan–Meier analysis showed that the 121-gene set classifier can separate significantly low- and high-risk groups in the 13 major TCGA cancers. Related to Figure 9.** The Kaplan–Meier curves of the TCGA cancer types of (A) LUSC, (B) STAD, (C) glioma, (D) BRCA were shown in this figure.

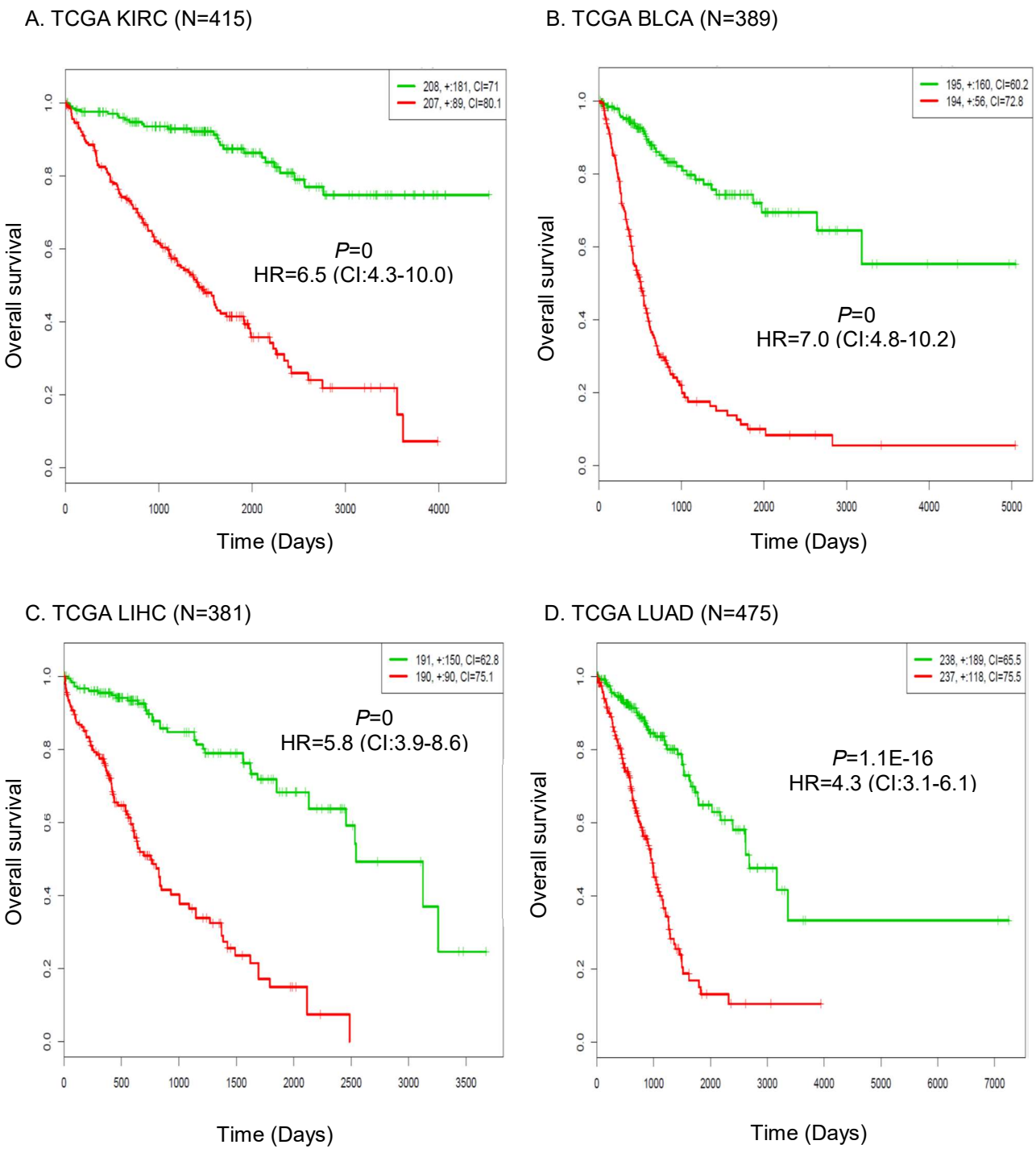


**Figure S11. Kaplan–Meier analysis showed that the 121-gene set classifier can separate significantly low- and high-risk groups in the 13 major TCGA cancers. Related to Figure 9.** The Kaplan–Meier curves of the TCGA cancer types of (A) KIRC, (B) BLCA, (C) LIHC, (D) LUAD were shown in this figure.

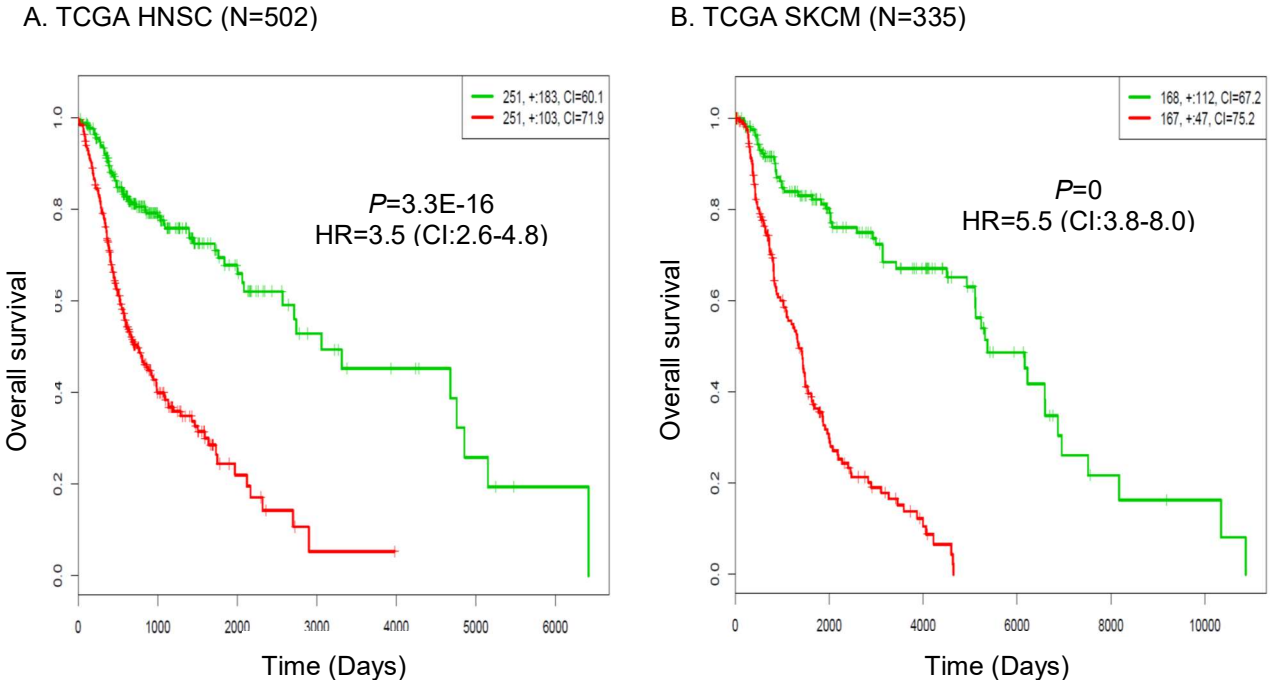


**Figure S12. Kaplan–Meier analysis showed that the 121-gene set classifier can separate significantly low- and high-risk groups in the 13 major TCGA cancers. Related to Figure 9.** The Kaplan–Meier curves of the TCGA cancer types of (A) HNSC, (B) SKCM were shown in this figure.

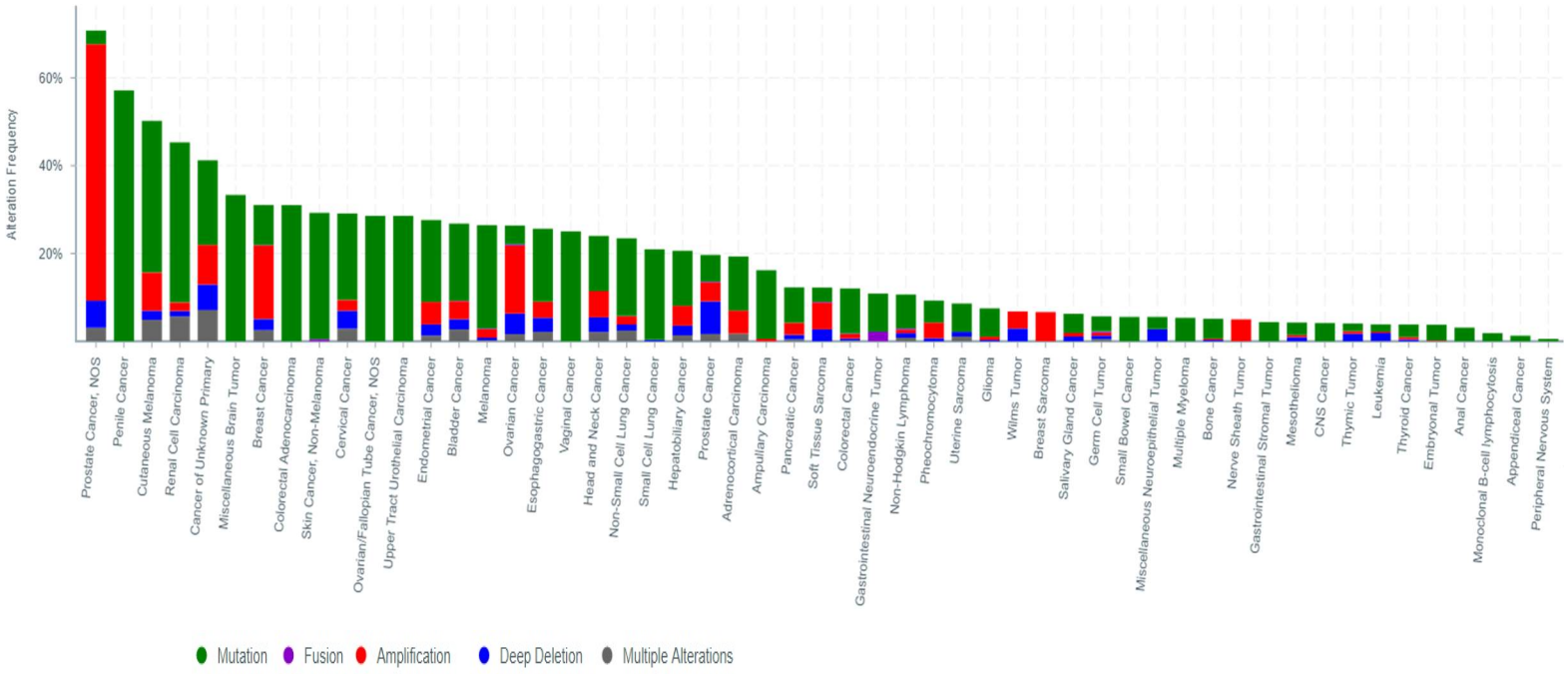


**Figure S13. The mutation analysis highlighted eleven genes with deleterious mutations in the HPD tumors after anti-PD-1 therapy. Related to Table 2.** Most of these genes have not been adequately studied in the cancer context before. Querying the HPD tumors associated 11-mutated-gene set in the cBioPortal website (http://www.cbioportal.org/) showed that this gene set had somatic mutations or copy number aberrations (CNAs) in 8887 (22%) of 41320 sequenced patients. The frequencies of tumor samples having somatic alterations in at least one of the eleven genes among each type of cancers archived in cBioPortal were shown in the figure.

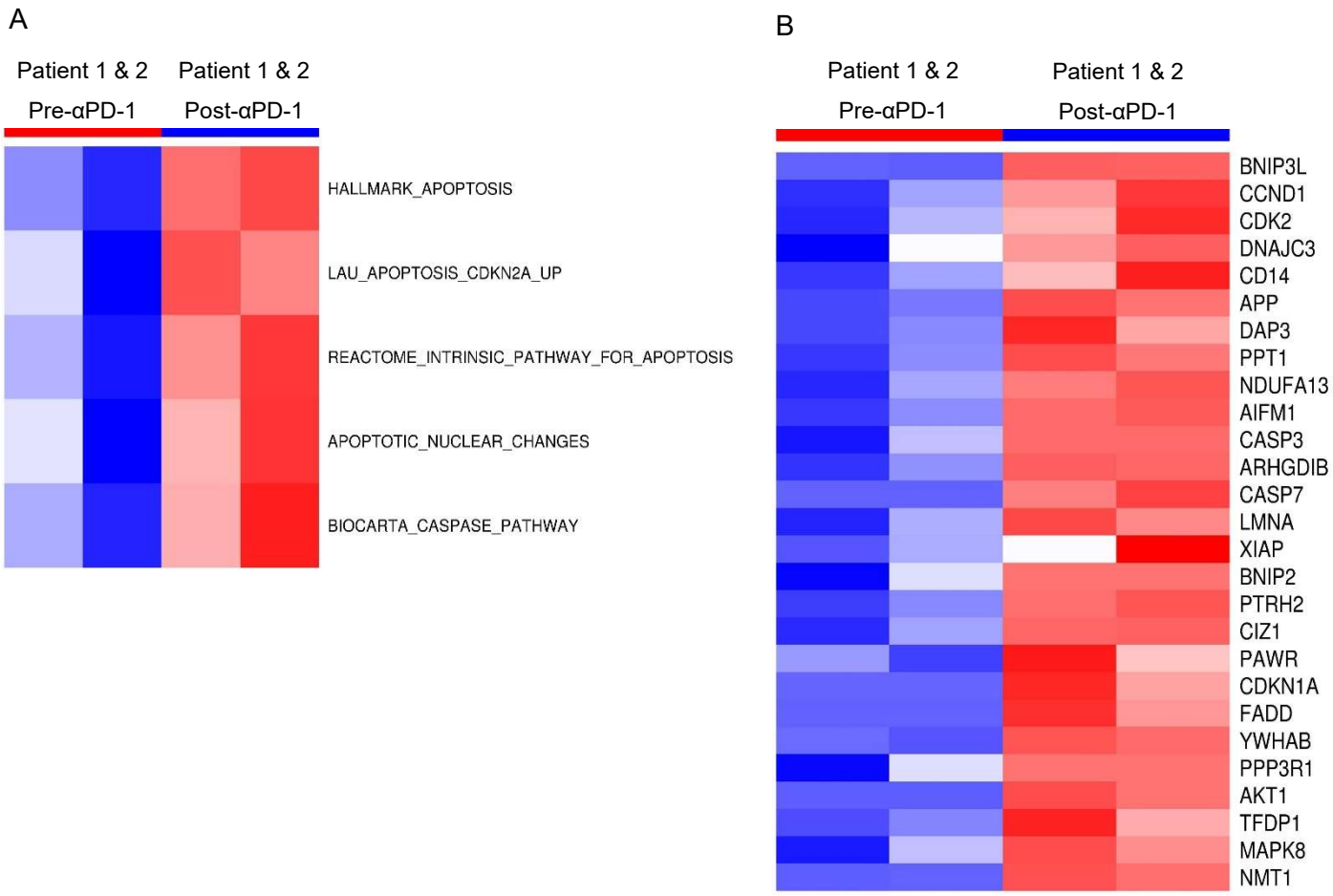


**Figure S14. Changes of the apoptosis pathway activity in the after anti-PD-1 immunotherapy tumors of the HPD patients. Related to Figure 5 and Figure 6.** (A) Five apoptosis gene sets were activated in the two patients after anti-PD-1 immunotherapy; (B) 27 apoptotic genes of these five apoptosis gene sets including marker genes in caspase/bcl2 pathways (CASP3, CASP7, BNIP2, BNIP3L) were significantly up-regulated.

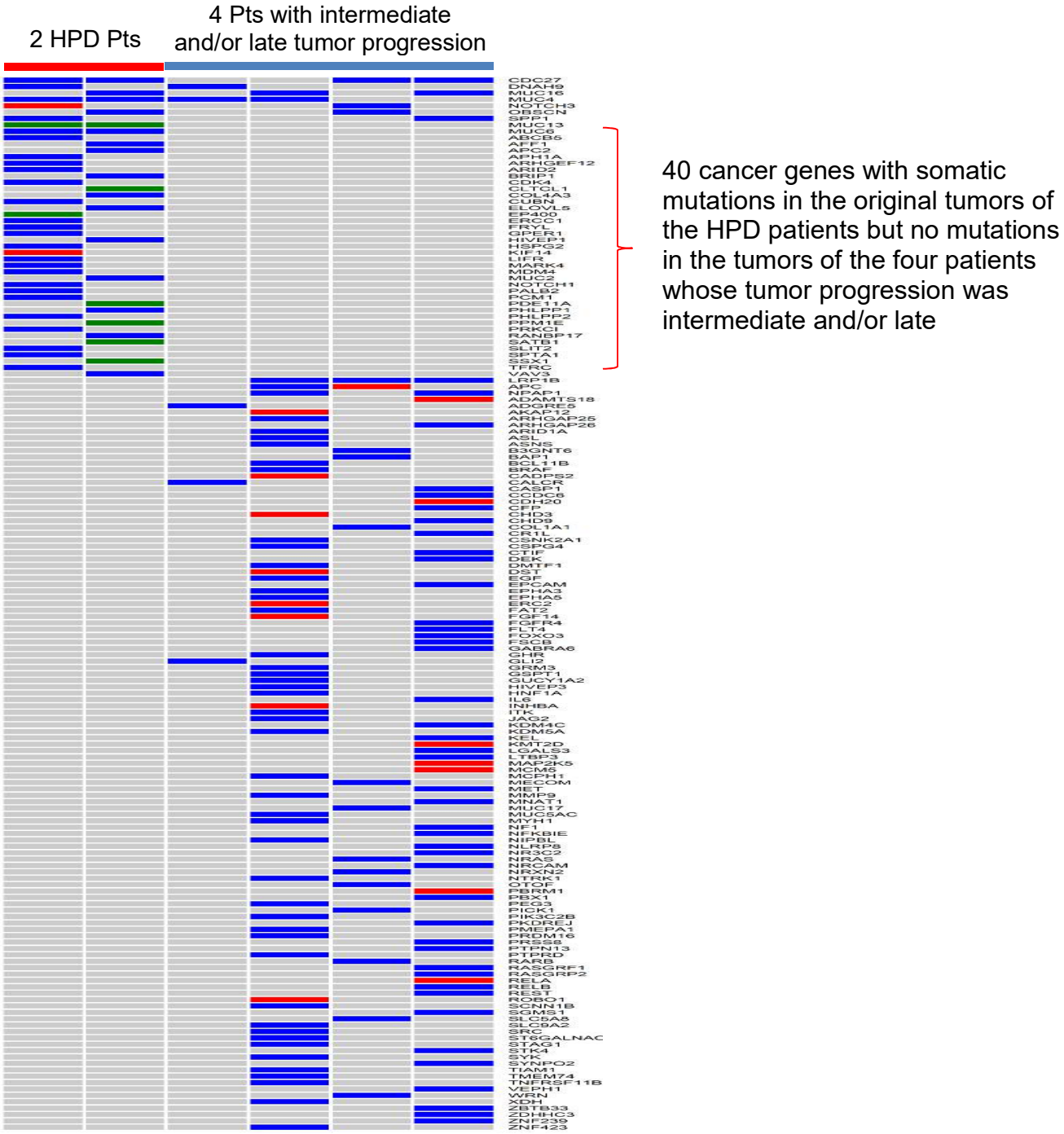


**Figure S15. Comparison of the somatic mutation profiles of pretreatment tumor samples between HPD patients and a subset of non-HPD patients. Related to Figure 9.** Mutation analysis showed that 40 cancer genes had somatic mutations in the original tumors of the HPD patients but no mutations in the tumors of the patients whose tumor progression was intermediate and/or late.

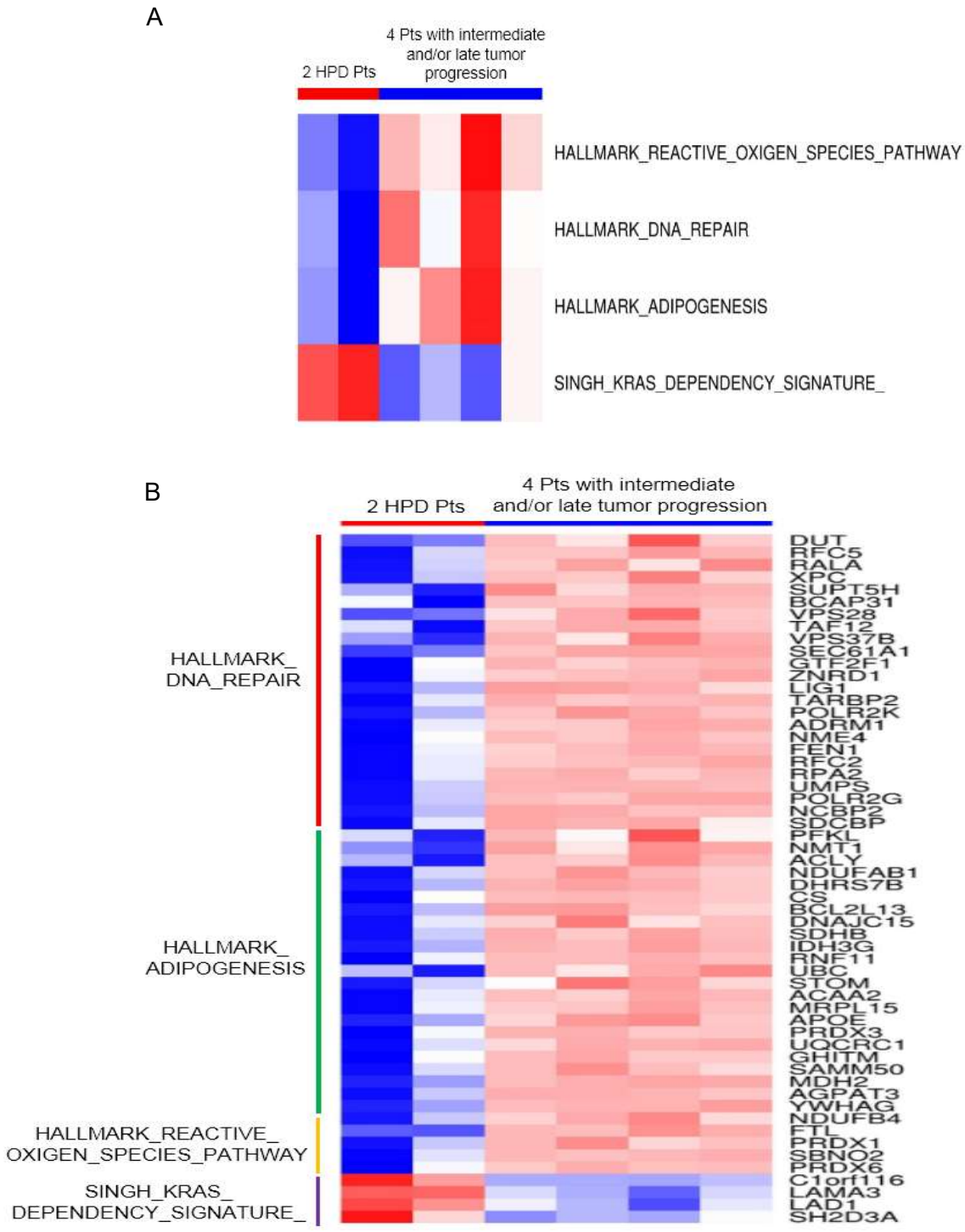


**Figure S16. GSVA analysis of the transcriptional profiles of pretreatment tumor samples between HPD patients and a subset of non-HPD patients. Related to Figure 9.** (A) Four gene sets were significantly altered in the tumors of HPD patients compared to the patients with intermediate and/or late tumor progression; (B) The corresponding gene expression changes of the above significantly altered pathways were also shown.

**Table S1, Table S2, Table S3 were the supplemental Excel files.**

**Table S4. The clinical information of the eighteen follicular lymphoma patients from the GSE52562 study, among whom two patients had PFS less than two months together with advanced tumor progression phenotypes after anti-PD-1 treatment. Related to Figure 9.**

| ExpId | SampleID | gender | age | pfs.censorship | pfs.time.month | treatment | tissue | HPDstatus |
|---|---|---|---|---|---|---|---|---|
| GSM1269893 | SAMPLE.25 | F | 67 | 1 | 1.8 | pre-pidilizumab | tumor biopsy | HPD |
| GSM1269873 | SAMPLE.5 | F | 79 | 1 | 2.0 | pre-pidilizumab | tumor biopsy | HPD |
| GSM1269883 | SAMPLE.15 | M | 46 | 1 | 3.7 | pre-pidilizumab | tumor biopsy | nonHPD |
| GSM1269886 | SAMPLE.18 | M | 69 | 0 | 4.1 | pre-pidilizumab | tumor biopsy | nonHPD |
| GSM1269877 | SAMPLE.9 | F | 58 | 1 | 6.5 | pre-pidilizumab | tumor biopsy | nonHPD |
| GSM1269888 | SAMPLE.20 | F | 56 | 0 | 7.1 | pre-pidilizumab | tumor biopsy | nonHPD |
| GSM1269875 | SAMPLE.7 | M | 60 | 1 | 10.1 | pre-pidilizumab | tumor biopsy | nonHPD |
| GSM1269889 | SAMPLE.21 | F | 62 | 1 | 12.7 | pre-pidilizumab | tumor biopsy | nonHPD |
| GSM1269871 | SAMPLE.3 | M | 51 | 1 | 13.5 | pre-pidilizumab | tumor biopsy | nonHPD |
| GSM1269894 | SAMPLE.26 | M | 58 | 1 | 15.3 | pre-pidilizumab | tumor biopsy | nonHPD |
| GSM1269890 | SAMPLE.22 | M | 70 | 1 | 18.6 | pre-pidilizumab | tumor biopsy | nonHPD |
| GSM1269892 | SAMPLE.24 | M | 63 | 0 | 18.8 | pre-pidilizumab | tumor biopsy | nonHPD |
| GSM1269879 | SAMPLE.11 | M | 67 | 1 | 19.6 | pre-pidilizumab | tumor biopsy | nonHPD |
| GSM1269869 | SAMPLE.1 | F | 61 | 1 | 21.6 | pre-pidilizumab | tumor biopsy | nonHPD |
| GSM1269891 | SAMPLE.23 | F | 37 | 0 | 26.5 | pre-pidilizumab | tumor biopsy | nonHPD |
| GSM1269887 | SAMPLE.19 | F | 41 | 0 | 30.4 | pre-pidilizumab | tumor biopsy | nonHPD |
| GSM1269881 | SAMPLE.13 | M | 58 | 0 | 30.8 | pre-pidilizumab | tumor biopsy | nonHPD |
| GSM1269885 | SAMPLE.17 | F | 45 | 0 | 35.0 | pre-pidilizumab | tumor biopsy | nonHPD |

**Table S5. The information of the 121 genes in the expression signature of pre-anti-PD-1 treatment tumors that may be predictive of HPD (hyperprogressive disease) patients after anti-PD-1 immunotherapy. Related to Figure 9.**

| Gene Symbol | Entrez Gene Name | Location | Type(s) |
|---|---|---|---|
| AAK1 | AP2 associated kinase 1 | Cytoplasm | kinase |
| ACOT1 | acyl-CoA thioesterase 1 | Cytoplasm | enzyme |
| ACOT2 | acyl-CoA thioesterase 2 | Cytoplasm | enzyme |
| ADAR | adenosine deaminase, RNA specific | Nucleus | enzyme |
| AFF1 | AF4/FMR2 family member 1 | Nucleus | transcription regulator |
| ANKS6 | ankyrin repeat and sterile alpha motif domain containing 6 | Cytoplasm | other |
| ANXA5 | annexin A5 | Plasma Membrane | transporter |
| ARID2 | AT-rich interaction domain 2 | Nucleus | transcription regulator |

| | | | |
|---|---|---|---|
| ARL1 | ADP ribosylation factor like GTPase 1 | Cytoplasm | enzyme |
| ARMC9 | armadillo repeat containing 9 | Cytoplasm | other |
| ATF7IP | activating transcription factor 7 interacting protein | Nucleus | transcription regulator |
| ATP11C | ATPase phospholipid transporting 11C | Plasma Membrane | transporter |
| ATP5L | ATP synthase membrane subunit g | Cytoplasm | enzyme |
| BAZ1B | bromodomain adjacent to zinc finger domain 1B | Nucleus | transcription regulator |
| BAZ2A | bromodomain adjacent to zinc finger domain 2A | Nucleus | transcription regulator |
| C17orf97 | chromosome 17 open reading frame 97 | Other | other |
| CAMSAP1 | calmodulin regulated spectrin associated protein 1 | Cytoplasm | other |
| CARD8 | caspase recruitment domain family member 8 | Nucleus | other |
| CCNA1 | cyclin A1 | Nucleus | other |
| CCNT1 | cyclin T1 | Nucleus | transcription regulator |
| CD63 | CD63 molecule | Plasma Membrane | other |
| CD96 | CD96 molecule | Plasma Membrane | other |
| CHD4 | chromodomain helicase DNA binding protein 4 | Nucleus | enzyme |
| CLSTN3 | calsyntenin 3 | Plasma Membrane | other |
| COL4A1 | collagen type IV alpha 1 chain | Extracellular Space | other |
| COL4A2 | collagen type IV alpha 2 chain | Extracellular Space | other |
| COMMD9 | COMM domain containing 9 | Cytoplasm | other |
| CORO1C | coronin 1C | Cytoplasm | other |
| CPT1A | carnitine palmitoyltransferase 1A | Cytoplasm | enzyme |
| CREBZF | CREB/ATF bZIP transcription factor | Nucleus | transcription regulator |
| CSNK1G1 | casein kinase 1 gamma 1 | Cytoplasm | kinase |
| CTLA4 | cytotoxic T-lymphocyte associated protein 4 | Plasma Membrane | transmembrane receptor |
| CYP2D6 | cytochrome P450 family 2 subfamily D member 6 | Cytoplasm | enzyme |
| DGKD | diacylglycerol kinase delta | Cytoplasm | kinase |
| DIAPH1 | diaphanous related formin 1 | Plasma Membrane | other |
| EID2 | EP300 interacting inhibitor of differentiation 2 | Nucleus | other |
| ELK4 | ELK4, ETS transcription factor | Nucleus | transcription regulator |
| EP300 | E1A binding protein p300 | Nucleus | transcription regulator |
| ERN1 | endoplasmic reticulum to nucleus signaling 1 | Cytoplasm | kinase |
| FAHD1 | fumarylacetoacetate hydrolase domain containing 1 | Cytoplasm | enzyme |
| FAM104B | family with sequence similarity 104 member B | Other | other |
| FBXL17 | F-box and leucine rich repeat protein 17 | Other | other |

| | | | |
|---|---|---|---|
| FPGT | fucose-1-phosphate guanylyltransferase | Cytoplasm | enzyme |
| FUBP3 | far upstream element binding protein 3 | Nucleus | transcription regulator |
| FUCA2 | alpha-L-fucosidase 2 | Extracellular Space | enzyme |
| GALNT10 | polypeptide N-acetylgalactosaminyltransferase 10 | Cytoplasm | enzyme |
| GALNT2 | polypeptide N-acetylgalactosaminyltransferase 2 | Cytoplasm | enzyme |
| GAPVD1 | GTPase activating protein and VPS9 domains 1 | Cytoplasm | other |
| GATAD2B | GATA zinc finger domain containing 2B | Nucleus | transcription regulator |
| GBF1 | golgi brefeldin A resistant guanine nucleotide exchange factor 1 | Cytoplasm | other |
| GOLIM4 | golgi integral membrane protein 4 | Cytoplasm | other |
| GPR18 | G protein-coupled receptor 18 | Plasma Membrane | G-protein coupled receptor |
| HADH | hydroxyacyl-CoA dehydrogenase | Cytoplasm | enzyme |
| HHLA3 | HERV-H LTR-associating 3 | Other | other |
| HIVEP1 | human immunodeficiency virus type I enhancer binding protein 1 | Nucleus | transcription regulator |
| HIVEP2 | human immunodeficiency virus type I enhancer binding protein 2 | Nucleus | transcription regulator |
| HMBS | hydroxymethylbilane synthase | Cytoplasm | enzyme |
| HPGDS | hematopoietic prostaglandin D synthase | Cytoplasm | enzyme |
| HSPG2 | heparan sulfate proteoglycan 2 | Extracellular Space | enzyme |
| KDM6B | lysine demethylase 6B | Extracellular Space | enzyme |
| KDR | kinase insert domain receptor | Plasma Membrane | kinase |
| KLHDC8B | kelch domain containing 8B | Cytoplasm | other |
| LAMTOR3 | late endosomal/lysosomal adaptor, MAPK and MTOR activator 3 | Cytoplasm | other |
| LGALS12 | galectin 12 | Extracellular Space | other |
| LNPEP | leucyl and cystinyl aminopeptidase | Cytoplasm | peptidase |
| LRP6 | LDL receptor related protein 6 | Plasma Membrane | transmembrane receptor |
| MAGEH1 | MAGE family member H1 | Cytoplasm | other |
| MEF2D | myocyte enhancer factor 2D | Nucleus | transcription regulator |
| MTIF3 | mitochondrial translational initiation factor 3 | Cytoplasm | translation regulator |
| NFE2L2 | nuclear factor, erythroid 2 like 2 | Nucleus | transcription regulator |
| NOTCH3 | notch 3 | Plasma Membrane | transcription regulator |
| NPLOC4 | NPL4 homolog, ubiquitin recognition factor | Nucleus | other |
| NSD1 | nuclear receptor binding SET domain protein 1 | Nucleus | transcription regulator |
| NUP188 | nucleoporin 188 | Nucleus | other |
| OBSCN | obscurin, cytoskeletal calmodulin and titin-interacting RhoGEF | Cytoplasm | kinase |
| OTUD7B | OTU deubiquitinase 7B | Cytoplasm | peptidase |

| | | | |
|---|---|---|---|
| PAK2 | p21 (RAC1) activated kinase 2 | Cytoplasm | kinase |
| PCDHGB7 | protocadherin gamma subfamily B, 7 | Other | other |
| PHF8 | PHD finger protein 8 | Nucleus | enzyme |
| PPM1L | protein phosphatase, Mg2+/Mn2+ dependent 1L | Cytoplasm | phosphatase |
| PPP2R3C | protein phosphatase 2 regulatory subunit B''gamma | Cytoplasm | other |
| PTPN3 | protein tyrosine phosphatase, non-receptor type 3 | Cytoplasm | phosphatase |
| PTS | 6-pyruvoyltetrahydropterin synthase | Cytoplasm | enzyme |
| RANGAP1 | Ran GTPase activating protein 1 | Nucleus | other |
| SATB1 | SATB homeobox 1 | Nucleus | transcription regulator |
| SERPINF1 | serpin family F member 1 | Extracellular Space | other |
| SETX | senataxin | Nucleus | enzyme |
| SLC25A34 | solute carrier family 25 member 34 | Cytoplasm | other |
| SLC27A1 | solute carrier family 27 member 1 | Plasma Membrane | transporter |
| SLC38A6 | solute carrier family 38 member 6 | Plasma Membrane | transporter |
| SLC6A6 | solute carrier family 6 member 6 | Plasma Membrane | transporter |
| SMURF1 | SMAD specific E3 ubiquitin protein ligase 1 | Cytoplasm | enzyme |
| SNAPC4 | small nuclear RNA activating complex polypeptide 4 | Nucleus | transcription regulator |
| SORT1 | sortilin 1 | Plasma Membrane | G-protein coupled receptor |
| SPEN | spen family transcriptional repressor | Nucleus | transcription regulator |
| SPIN2A | spindlin family member 2A | Other | other |
| SPP1 | secreted phosphoprotein 1 | Extracellular Space | cytokine |
| SSBP2 | single stranded DNA binding protein 2 | Nucleus | transcription regulator |
| OBFC1 | STN1, CST complex subunit | Nucleus | other |
| SYTL4 | synaptotagmin like 4 | Cytoplasm | transporter |
| TCF4 | transcription factor 4 | Nucleus | transcription regulator |
| TEX261 | testis expressed 261 | Extracellular Space | other |
| TGOLN2 | trans-golgi network protein 2 | Cytoplasm | other |
| TIMM8B | translocase of inner mitochondrial membrane 8 homolog B | Cytoplasm | transporter |
| TLN1 | talin 1 | Plasma Membrane | other |
| TMEM99 | transmembrane protein 99 | Other | other |
| TNFRSF25 | TNF receptor superfamily member 25 | Plasma Membrane | transmembrane receptor |
| TNKS2 | tankyrase 2 | Nucleus | enzyme |
| TRIO | trio Rho guanine nucleotide exchange factor | Cytoplasm | kinase |
| TRIP12 | thyroid hormone receptor interactor 12 | Cytoplasm | enzyme |
| TSC2 | TSC complex subunit 2 | Cytoplasm | other |
| TSPAN3 | tetraspanin 3 | Plasma Membrane | other |

| | | | |
|---|---|---|---|
| UBTF | upstream binding transcription factor, RNA polymerase I | Nucleus | transcription regulator |
| KIAA2018 | upstream transcription factor family member 3 | Other | other |
| VHL | von Hippel-Lindau tumor suppressor | Nucleus | transcription regulator |
| WDR44 | WD repeat domain 44 | Cytoplasm | other |
| YWHAE | tyrosine 3-monooxygenase/tryptophan 5-monooxygenase activation protein epsilon | Cytoplasm | other |
| YWHAQ | tyrosine 3-monooxygenase/tryptophan 5-monooxygenase activation protein theta | Cytoplasm | other |
| ZFP36L1 | ZFP36 ring finger protein like 1 | Nucleus | transcription regulator |
| ZNF609 | zinc finger protein 609 | Nucleus | other |
| ZNF878 | zinc finger protein 878 | Other | other |

**Table S6. The clinical information of the 51 melanoma patients subjected to nivolumab immunotherapy from the CA209-038 study, among whom 21 patients had PFS less than two months together with post-therapy tumor progression phenotypes. Related to Figure 9.**

| PatientID | Sample | SampleType | PFS Censorship | Clinical Phenotype | PFS (days) | HPD status |
|---|---|---|---|---|---|---|
| Pt103 | Pt103_Pre | Pre-anti-PD-1 tumor | 0 | PROGRESSION | 50 | HPD |
| Pt106 | Pt106_Pre | Pre-anti-PD-1 tumor | 0 | PROGRESSION | 56 | HPD |
| Pt11 | Pt11_Pre | Pre-anti-PD-1 tumor | 0 | PROGRESSION | 59 | HPD |
| Pt17 | Pt17_Pre | Pre-anti-PD-1 tumor | 0 | PROGRESSION | 48 | HPD |
| Pt1 | Pt1_Pre | Pre-anti-PD-1 tumor | 0 | PROGRESSION | 54 | HPD |
| Pt24 | Pt24_Pre | Pre-anti-PD-1 tumor | 0 | PROGRESSION | 50 | HPD |
| Pt27 | Pt27_Pre | Pre-anti-PD-1 tumor | 0 | PROGRESSION | 50 | HPD |
| Pt29 | Pt29_Pre | Pre-anti-PD-1 tumor | 0 | PROGRESSION | 50 | HPD |
| Pt31 | Pt31_Pre | Pre-anti-PD-1 tumor | 0 | PROGRESSION | 50 | HPD |
| Pt39 | Pt39_Pre | Pre-anti-PD-1 tumor | 0 | PROGRESSION | 57 | HPD |
| Pt46 | Pt46_Pre | Pre-anti-PD-1 tumor | 0 | PROGRESSION | 51 | HPD |
| Pt47 | Pt47_Pre | Pre-anti-PD-1 tumor | 0 | PROGRESSION | 57 | HPD |
| Pt52 | Pt52_Pre | Pre-anti-PD-1 tumor | 0 | PROGRESSION | 57 | HPD |
| Pt5 | Pt5_Pre | Pre-anti-PD-1 tumor | 0 | PROGRESSION | 56 | HPD |
| Pt62 | Pt62_Pre | Pre-anti-PD-1 tumor | 0 | PROGRESSION | 56 | HPD |
| Pt66 | Pt66_Pre | Pre-anti-PD-1 tumor | 0 | PROGRESSION | 59 | HPD |
| Pt78 | Pt78_Pre | Pre-anti-PD-1 tumor | 0 | PROGRESSION | 50 | HPD |
| Pt84 | Pt84_Pre | Pre-anti-PD-1 tumor | 0 | PROGRESSION | 50 | HPD |
| Pt85 | Pt85_Pre | Pre-anti-PD-1 tumor | 0 | PROGRESSION | 49 | HPD |
| Pt8 | Pt8_Pre | Pre-anti-PD-1 tumor | 0 | PROGRESSION | 52 | HPD |
| Pt90 | Pt90_Pre | Pre-anti-PD-1 tumor | 0 | PROGRESSION | 44 | HPD |
| Pt101 | Pt101_Pre | Pre-anti-PD-1 tumor | 0 | PARTIAL RESPONSE | 612 | nonHPD |
| Pt10 | Pt10_Pre | Pre-anti-PD-1 tumor | 0 | STABLE DISEASE | 119 | nonHPD |
| Pt18 | Pt18_Pre | Pre-anti-PD-1 tumor | 0 | NA | 519 | nonHPD |
| Pt23 | Pt23_Pre | Pre-anti-PD-1 tumor | 0 | DEATH PRIOR TO DISEASE ASSESSMENT | 52 | nonHPD |
| Pt26 | Pt26_Pre | Pre-anti-PD-1 tumor | 0 | PROGRESSION | 294 | nonHPD |
| Pt28 | Pt28_Pre | Pre-anti-PD-1 tumor | 0 | PROGRESSION | 61 | nonHPD |
| Pt2 | Pt2_Pre | Pre-anti-PD-1 tumor | 1 | STABLE DISEASE | 115 | nonHPD |
| Pt30 | Pt30_Pre | Pre-anti-PD-1 tumor | 0 | PARTIAL RESPONSE | 603 | nonHPD |
| Pt34 | Pt34_Pre | Pre-anti-PD-1 tumor | 1 | NA | 834 | nonHPD |
| Pt36 | Pt36_Pre | Pre-anti-PD-1 tumor | 1 | NA | 737 | nonHPD |
| Pt37 | Pt37_Pre | Pre-anti-PD-1 tumor | 0 | STABLE DISEASE | 176 | nonHPD |
| Pt38 | Pt38_Pre | Pre-anti-PD-1 tumor | 0 | PROGRESSION | 167 | nonHPD |
| Pt3 | Pt3_Pre | Pre-anti-PD-1 tumor | 0 | PARTIAL RESPONSE | 583 | nonHPD |
| Pt44 | Pt44_Pre | Pre-anti-PD-1 tumor | 0 | PARTIAL RESPONSE | 560 | nonHPD |
| Pt48 | Pt48_Pre | Pre-anti-PD-1 tumor | 1 | NA | 1046 | nonHPD |
| Pt49 | Pt49_Pre | Pre-anti-PD-1 tumor | 1 | PARTIAL RESPONSE | 827 | nonHPD |
| Pt4 | Pt4_Pre | Pre-anti-PD-1 tumor | 0 | STABLE DISEASE | 175 | nonHPD |
| Pt59 | Pt59_Pre | Pre-anti-PD-1 tumor | 0 | STABLE DISEASE | 111 | nonHPD |
| Pt65 | Pt65_Pre | Pre-anti-PD-1 tumor | 1 | STABLE DISEASE | 280 | nonHPD |
| Pt67 | Pt67_Pre | Pre-anti-PD-1 tumor | 0 | STABLE DISEASE | 281 | nonHPD |
| Pt72 | Pt72_Pre | Pre-anti-PD-1 tumor | 0 | PARTIAL RESPONSE | 333 | nonHPD |
| Pt76 | Pt76_Pre | Pre-anti-PD-1 tumor | 0 | NA | 10 | nonHPD |

| | | | | | | |
|---|---|---|---|---|---|---|
| Pt77 | Pt77_Pre | Pre-anti-PD-1 tumor | 0 | STABLE DISEASE | 163 | nonHPD |
| Pt79 | Pt79_Pre | Pre-anti-PD-1 tumor | 0 | STABLE DISEASE | 171 | nonHPD |
| Pt82 | Pt82_Pre | Pre-anti-PD-1 tumor | 0 | STABLE DISEASE | 220 | nonHPD |
| Pt89 | Pt89_Pre | Pre-anti-PD-1 tumor | 0 | STABLE DISEASE | 219 | nonHPD |
| Pt92 | Pt92_Pre | Pre-anti-PD-1 tumor | 0 | STABLE DISEASE | 190 | nonHPD |
| Pt94 | Pt94_Pre | Pre-anti-PD-1 tumor | 1 | COMPLETE RESPONSE | 729 | nonHPD |
| Pt98 | Pt98_Pre | Pre-anti-PD-1 tumor | 0 | STABLE DISEASE | 408 | nonHPD |
| Pt9 | Pt9_Pre | Pre-anti-PD-1 tumor | 0 | PROGRESSION | 66 | nonHPD |

**Table S7. The information of the 40 HPD associated cancer genes having nonsilent somatic mutations in the original tumors of the HPD patients but no mutations in the tumors of the patients whose tumor progression was intermediate and/or late. Related to Figure 9.**

| Symbol | Entrez Gene Name | Location | Type(s) |
|---|---|---|---|
| ABCB5 | ATP binding cassette subfamily B member 5 | Plasma Membrane | transporter |
| AFF1 | AF4/FMR2 family member 1 | Nucleus | transcription regulator |
| APC2 | APC2, WNT signaling pathway regulator | Cytoplasm | enzyme |
| APH1A | aph-1 homolog A, gamma-secretase subunit | Cytoplasm | peptidase |
| ARHGEF12 | Rho guanine nucleotide exchange factor 12 | Cytoplasm | other |
| ARID2 | AT-rich interaction domain 2 | Nucleus | transcription regulator |
| BRIP1 | BRCA1 interacting protein C-terminal helicase 1 | Nucleus | enzyme |
| CDK4 | cyclin dependent kinase 4 | Nucleus | kinase |
| CLTCL1 | clathrin heavy chain like 1 | Plasma Membrane | other |
| COL4A3 | collagen type IV alpha 3 chain | Extracellular Space | other |
| CUBN | cubilin | Plasma Membrane | transmembrane receptor |
| ELOVL5 | ELOVL fatty acid elongase 5 | Cytoplasm | enzyme |
| EP400 | E1A binding protein p400 | Nucleus | other |
| ERCC1 | ERCC excision repair 1, endonuclease non-catalytic subunit | Nucleus | enzyme |
| FRYL | FRY like transcription coactivator | Other | other |
| GPER1 | G protein-coupled estrogen receptor 1 | Plasma Membrane | G-protein coupled receptor |
| HIVEP1 | human immunodeficiency virus type I enhancer binding protein 1 | Nucleus | transcription regulator |
| HSPG2 | heparan sulfate proteoglycan 2 | Extracellular Space | enzyme |
| KIF14 | kinesin family member 14 | Cytoplasm | enzyme |
| LIFR | LIF receptor alpha | Plasma Membrane | transmembrane receptor |
| MARK4 | microtubule affinity regulating kinase 4 | Cytoplasm | kinase |
| MDM4 | MDM4, p53 regulator | Nucleus | enzyme |
| MUC13 | mucin 13, cell surface associated | Extracellular Space | other |
| MUC2 | mucin 2, oligomeric mucus/gel-forming | Extracellular Space | other |
| MUC6 | mucin 6, oligomeric mucus/gel-forming | Extracellular Space | other |
| NOTCH1 | notch 1 | Plasma Membrane | transcription regulator |
| PALB2 | partner and localizer of BRCA2 | Nucleus | other |
| PCM1 | pericentriolar material 1 | Cytoplasm | other |
| PDE11A | phosphodiesterase 11A | Cytoplasm | enzyme |
| PHLPP1 | PH domain and leucine rich repeat protein phosphatase 1 | Cytoplasm | enzyme |
| PHLPP2 | PH domain and leucine rich repeat protein phosphatase 2 | Cytoplasm | enzyme |
| PPM1E | protein phosphatase, Mg2+/Mn2+ dependent 1E | Nucleus | phosphatase |
| PRKCI | protein kinase C iota | Cytoplasm | kinase |
| RANBP17 | RAN binding protein 17 | Nucleus | transporter |
| SATB1 | SATB homeobox 1 | Nucleus | transcription regulator |
| SLIT2 | slit guidance ligand 2 | Extracellular Space | other |
| SPTA1 | spectrin alpha, erythrocytic 1 | Cytoplasm | other |
| SSX1 | SSX family member 1 | Nucleus | transcription regulator |
| TFRC | transferrin receptor | Plasma Membrane | transporter |
| VAV3 | vav guanine nucleotide exchange factor 3 | Extracellular Space | cytokine |

**Transparent Methods**:

**Whole-exome sequencing (WES) and RNA-seq experimentation and data analyses**

For each set of paired tumor samples, a section of formalin-fixed tissue was examined with hematoxylin and eosin (H&E) staining to confirm the presence of tumor and determine the relative tumor burden. At least five 10-mm FFPE slides were used for each tumor specimen, from which DNA and RNA were purified by a commercial vendor (Omega Bio-tek, Inc., Norcross, GA 30071) and subjected to WES and RNA-seq after library purification. The Illumina Nextera Rapid Capture Exome kit was used for the preparation of exome libraries, which were sequenced to the average depth of 150 X coverage in the paired end 150 bp (PE150) mode with a HiSeq 4000 system. The Illumina TruSeq RNA Access kit was used for the preparation of total RNA libraries that were sequenced to the average depth of 75 million reads in the paired end 100 bp (PE100) mode using the HiSeq 2500 system.

The WES short reads were aligned to a reference genome (NCBI human genome assembly hg19) using the BWA (Burrows-Wheeler Aligner) program (Li and Durbin, 2009). Each alignment was assigned a mapping quality score by BWA (Li and Durbin, 2009), which generated a Phred-scaled probability that the alignment is correct. Reads with low mapping quality scores (< 5) were removed to reduce the false positive rate. The PCR duplicates were detected and removed using Picard software. Local realignment of the BWA-aligned reads was performed using the Genome Analysis Toolkit (GATK) (McKenna et al., 2010). VarScan 2 (Koboldt et al., 2012) was used to identify somatic variants based on the local realignment results comparing each tumor with the two reference blood samples. Default parameters in VarScan 2 were used. The lists of shared SNVs/indels were then annotated using ANNOVAR (Wang et al., 2010). Single nucleotide polymorphisms (SNPs) were filtered against dbSNP version 142 (dbSNP 142). Plots of mutations were generated using the “oncoPrint” function provided by the R package – ComplexHeatmap (Gu et al., 2016). To identify somatic mutations with the most significant functional consequences, we predicted the impact of the mutations on

HPD tumors using the bioinformatics programs SIFT, PolyPhen-2, and FATHMM according to our previous approaches (Xiong et al., 2015). Network analysis of the eleven genes having deleterious mutations in HPD tumors was performed and graphically depicted using Ingenuity Pathway Analysis software (IPA, QIAGEN Inc., https://www.qiagenbioinformatics.com/products/ingenuitypathway-analysis). Mapping of the p.Y1611S mutation to the 3D structure of the TSC2 protein was performed using MuPIT software (Niknafs et al., 2013). The bioinformatics tools SciClone (Miller et al., 2014) and Clonevol (Dang et al., 2017) were used to identify the clonal structures of the paired tumors of the two HPD patients. Plots of the clonal mutation clusters were generated using the fishplot software feature (Miller et al., 2016).

RNA-seq sample quality was analyzed using the FastQC program (http://www.bioinformatics.babraham.ac.uk/projects/fastqc/). Raw sequence data reads in fasta format were first processed through Perl scripts (Haas et al., 2013). Data were then refined by removing reads containing adapter, poly-N, or low-quality reads (Pei et al., 2016; Wang et al., 2015). All downstream analyses were based on refined data. The “rsem prepare reference” script of the RSEM package was used to generate reference transcript sequences by using the gene annotation file (GTF) format and the full genome sequence (FASTA) format of human GRCh37 assembly. All of the quality reads of different samples were mapped to generated reference transcript sequences using the Bowtie-2 program (Langmead et al., 2009) to determine the identity between cDNA sequences and corresponding genomic exons in regions of exact matches. The “rsem calculate expression” script of RSEM was used to analyze both the alignment of reads against reference transcript sequences and the calculation of relative abundances. Normalized gene expression values in TPM (Transcripts Per Kilobase Million) were used as input of the AltAnalyze software (Olsson et al., 2016) for differential gene expression analysis. FDR (False discovery rate) corrected *P*-values of less than 0.05 were used as criteria for significantly regulated genes.

To perform oncogenic pathway or network analysis, the list of differentially expressed genes between paired pre- and post-anti-PD-1 therapy tumors of the two patients was analyzed through the use of IPA. The GSVA (Gene Set Variation Analysis) (Hanzelmann et al., 2013) and GSEA (Gene Set Enrichment Analysis) (Subramanian et al., 2005) approaches were used to analyze the activity and enrichment of immune cell populations, respectively. GSEA analysis was performed for pre-ranked differentially expressed genes using the option 'GseaPreranked'. One thousand permutations were used to calculate significance. A gene set was considered to be significantly enriched in one of the two groups when the *P* value was lower than 0.05 and the FDR was lower than 0.25 for the corresponding gene set. For inflammatory pathway analysis, we performed a focused gene expression study by analyzing the changes of the inflammatory related genes included in the Hallmark gene set for inflammatory response named "HALLMARK_INFLAMMATORY_RESPONSE" downloaded from the MSigDB database (Liberzon et al., 2015; Liberzon et al., 2011). The GSVA approach (Hanzelmann et al., 2013) was used to characterize the activity of inflammation pathways in the post-anti-PD-1 treatment HPD tumors vs pre-treatment tumors. All heatmaps of gene expression were generated using the R package – heatmap3 (https://cran.r-project.org/web/packages/heatmap3/).

**Tumor immunogenicity analysis**

Immunogenicity of the pre-anti-PD-1 treatment tumors and post-treatment HPD tumors was analyzed using published criteria (Charoentong et al., 2017; Hakimi et al., 2016). The immunophenoscore (IPS) was calculated on an arbitrary 0–10 scale based on the sum of the weighted averaged Z score of the four categories shown in Figure 5 in accordance to the previous methods (Charoentong et al., 2017; Tappeiner et al., 2017). Briefly, the four categories include 20 single factors such as the presence of specific immune cell types along with the abundance of MHC molecules, or molecules known to act as immunoinhibitors or immunostimulators. For each determinant, a sample-wise Z score from gene expression data

was calculated. For the six cell types, an average Z score from the corresponding metagenes was calculated. The metagenes were defined previously as non-overlapping sets of genes that are representative for specific immune cell subpopulations and are not expressed in normal tissue (Charoentong et al., 2017). The detailed list of genes included in the metagenes were available from the same literature (Charoentong et al., 2017). The determinants were then divided into four categories—effector cells (activated CD4+ or CD8+ T cells and effector memory CD4+ T cells or CD8+ T cells), and suppressive cells (Tregs and MDSCs [myeloid-derived suppressor cells]), MHC-related molecules, and checkpoints or immunomodulators are color-coded in the outer part of the wheel (red: positive Z score, blue: negative Z score).

**Development and validation of an HPD classifier based on gene expression data**

Previously, no gene expression signature had been identified to predict which patients might develop HPD after receiving anti-PD-1 immunotherapy. To identify such predictors, we analyzed the publicly available gene expression data sets of the anti-PD-1 immunotherapy studies that may contain subsets of patients that acquired HPD. Similar to previous studies (Champiat et al., 2017; Kato et al., 2017; Saada-Bouzid et al., 2017), we defined HPD as (1) progression at first restaging on therapy, (2) increase in tumor size > 50%, and (3) >2-fold increase in tumor growth rate (TGR). Based on these criteria, we identified two cohorts in these datasets that received anti-PD-1 treatment and contained patients that developed putative HPD. The first study (Accession # “GSE52562” in the GEO database) performed gene expression profiling of tumor biopsies before and after pidilizumab (a humanized anti-PD-1 monoclonal antibody, also called “CT-011”) therapy in patients with relapsed follicular lymphoma (Westin et al., 2014). Previously, it was suggested that binding to PD-1 was the main driver for pidilizumab’s activity. Recent analyses show that pidilizumab binds to a hypoglycosylated /nonglycosylated form of PD-1 that is present on a distinct subpopulation of exhausted T cells (Fried et al., 2018). Nevertheless, multiple studies have shown that pidilizumab can affect PD-1 function either through binding or

other mechanisms, so pidilizumab treatment is still considered as anti-PD-1 therapy (Abdin et al., 2018; Benson et al., 2010; Jelinek and Hajek, 2016; Mkrtichyan et al., 2011; Rosenblatt et al., 2011; Westin et al., 2014). Two of eighteen follicular lymphoma patients from this study had PFS less than two months after anti-PD-1 treatment. These two patients were classified as HPD patients, while the other sixteen were non-HPD patients (Table S4). To develop an HPD-associated gene expression signature, the pre-therapy tumor expression data of our two HPD patients were combined with the pre-treatment tumor expression data of the two HPD patients and sixteen non-HPD patients from the GSE52562 study. This was used as the HPD signature discovery dataset (called “Dataset_1”). Another study (quoted as “CA209-038”) assessed transcriptome changes in tumors from the patients with advanced melanoma before and after nivolumab immunotherapy (Riaz et al., 2017). This CA209-038 study had 21 advanced melanoma patients having PFS < 2 months after anti-PD-1 immunotherapy. Therefore, these 21 patients were classified as the HPD patients while the other 31 patients were classified as non-HPD patients (Table S6). These 51 patients had pre-therapy gene expression data available, and this dataset was used as the validation dataset (called “Dataset_2”).

Based on the genome-wide expression data of Dataset_1 and Dataset_2, we developed and validated a 121-gene classifier using the *cancerclass* R package (Budczies et al., 2014). The performance of the 121-gene set as a classifier was evaluated with the use of receiver-operating-characteristic curves, calculation of AUC (Hanley and McNeil, 1982), and estimates of sensitivity and specificity implemented in the *cancerclass* R package (Jan et al., 2014). This classification protocol starts with a feature selection step and continues with nearest-centroid classification. Fisher’s exact test was used for categorical variables. All confidence intervals are reported as two-sided binomial 95% confidence intervals. Statistical analysis was performed with R software, version 3.2.3 (R Project for Statistical Computing). We also tested the prognostic performance of the 121-gene signature using gene expression data from the TCGA tumor samples in conjunction with the online biomarker validation tool and database –

SurvExpress (Aguirre-Gamboa et al., 2013). Specifically, Kaplan-Meier survival analyses were implemented to estimate the survival functions after the samples were classified into two risk groups according to their risk scores based on the 121-gene set. Differences in survival risk between the two risk groups were assessed using the Mantel-Haenszel log-rank test.

**Supplemental References**


Abdin, S.M., Zaher, D.M., Arafa, E.A., and Omar, H.A. (2018). Tackling Cancer Resistance by Immunotherapy: Updated Clinical Impact and Safety of PD-1/PD-L1 Inhibitors. Cancers (Basel) *10*.

Aguirre-Gamboa, R., Gomez-Rueda, H., Martinez-Ledesma, E., Martinez-Torteya, A., Chacolla-Huaringa, R., Rodriguez-Barrientos, A., Tamez-Pena, J.G., and Trevino, V. (2013). SurvExpress: an online biomarker validation tool and database for cancer gene expression data using survival analysis. PLoS One *8*, e74250.

Benson, D.M., Jr., Bakan, C.E., Mishra, A., Hofmeister, C.C., Efebera, Y., Becknell, B., Baiocchi, R.A., Zhang, J., Yu, J., Smith, M.K.*, et al.* (2010). The PD-1/PD-L1 axis modulates the natural killer cell versus multiple myeloma effect: a therapeutic target for CT-011, a novel monoclonal anti-PD-1 antibody. Blood *116*, 2286-2294.

Budczies, J., Kosztyla, D., Torne, C.V., Stenzinger, A., Darb-Esfahani, S., Dietel, M., and Denkert, C. (2014). cancerclass: An R Package for development and validation of diagnostic tests from high-dimensional molecular data. J Stat Software *59*, 1-19.

Champiat, S., Dercle, L., Ammari, S., Massard, C., Hollebecque, A., Postel-Vinay, S., Chaput, N., Eggermont, A., Marabelle, A., Soria, J.C.*, et al.* (2017). Hyperprogressive Disease Is a New Pattern of Progression in Cancer Patients Treated by Anti-PD-1/PD-L1. Clin Cancer Res *23*, 1920-1928.

Charoentong, P., Finotello, F., Angelova, M., Mayer, C., Efremova, M., Rieder, D., Hackl, H., and Trajanoski, Z. (2017). Pan-cancer Immunogenomic Analyses Reveal Genotype-Immunophenotype Relationships and Predictors of Response to Checkpoint Blockade. Cell Rep *18*, 248-262.

Dang, H.X., White, B.S., Foltz, S.M., Miller, C.A., Luo, J., Fields, R.C., and Maher, C.A. (2017). ClonEvol: clonal ordering and visualization in cancer sequencing. Ann Oncol *28*, 3076-3082.

Fried, I., Lossos, A., Ben Ami, T., Dvir, R., Toledano, H., Ben Arush, M.W., Postovski, S., Abu Kuidar, A., Yalon, M., Weintraub, M.*, et al.* (2018). Preliminary results of immune modulating antibody MDV9300 (pidilizumab) treatment in children with diffuse intrinsic pontine glioma. J Neurooncol *136*, 189-195.

Gu, Z., Eils, R., and Schlesner, M. (2016). Complex heatmaps reveal patterns and correlations in multidimensional genomic data. Bioinformatics *32*, 2847-2849.

Haas, B.J., Papanicolaou, A., Yassour, M., Grabherr, M., Blood, P.D., Bowden, J., Couger, M.B., Eccles, D., Li, B., Lieber, M.*, et al.* (2013). De novo transcript sequence reconstruction from RNA-seq using the Trinity platform for reference generation and analysis. Nat Protoc *8*, 1494-1512.

Hakimi, A.A., Reznik, E., Lee, C.H., Creighton, C.J., Brannon, A.R., Luna, A., Aksoy, B.A., Liu, E.M., Shen, R., Lee, W.*, et al.* (2016). An Integrated Metabolic Atlas of Clear Cell Renal Cell Carcinoma. Cancer Cell *29*, 104-116.

Hanley, J.A., and McNeil, B.J. (1982). The meaning and use of the area under a receiver operating characteristic (ROC) curve. Radiology *143*, 29-36.

Hanzelmann, S., Castelo, R., and Guinney, J. (2013). GSVA: gene set variation analysis for microarray and RNA-seq data. BMC Bioinformatics *14*, 7.

Jan, B., Kosztyla, D., von Törne, C., Stenzinger, A., Darb-Esfahani, S., Dietel, M., and Denkert, C. (2014). cancerclass: An R Package for Development and Validation of Diagnostic Tests from High-Dimensional Molecular Data. 2014 *59*, 19.

Jelinek, T., and Hajek, R. (2016). PD-1/PD-L1 inhibitors in multiple myeloma: The present and the future. Oncoimmunology *5*, e1254856.

Kato, S., Goodman, A., Walavalkar, V., Barkauskas, D.A., Sharabi, A., and Kurzrock, R. (2017). Hyperprogressors after Immunotherapy: Analysis of Genomic Alterations Associated with Accelerated Growth Rate. Clin Cancer Res *23*, 4242-4250.

Koboldt, D.C., Zhang, Q., Larson, D.E., Shen, D., McLellan, M.D., Lin, L., Miller, C.A., Mardis, E.R., Ding, L., and Wilson, R.K. (2012). VarScan 2: somatic mutation and copy number alteration discovery in cancer by exome sequencing. Genome Res *22*, 568-576.

Langmead, B., Trapnell, C., Pop, M., and Salzberg, S.L. (2009). Ultrafast and memory-efficient alignment of short DNA sequences to the human genome. Genome Biol *10*, R25.

Li, H., and Durbin, R. (2009). Fast and accurate short read alignment with Burrows-Wheeler transform. Bioinformatics *25*, 1754-1760.

Liberzon, A., Birger, C., Thorvaldsdottir, H., Ghandi, M., Mesirov, J.P., and Tamayo, P. (2015). The Molecular Signatures Database (MSigDB) hallmark gene set collection. Cell Syst *1*, 417-425.

Liberzon, A., Subramanian, A., Pinchback, R., Thorvaldsdottir, H., Tamayo, P., and Mesirov, J.P. (2011). Molecular signatures database (MSigDB) 3.0. Bioinformatics *27*, 1739-1740.

McKenna, A., Hanna, M., Banks, E., Sivachenko, A., Cibulskis, K., Kernytsky, A., Garimella, K., Altshuler, D., Gabriel, S., Daly, M.*, et al.* (2010). The Genome Analysis Toolkit: a MapReduce framework for analyzing next-generation DNA sequencing data. Genome Res *20*, 1297-1303.

Miller, C.A., McMichael, J., Dang, H.X., Maher, C.A., Ding, L., Ley, T.J., Mardis, E.R., and Wilson, R.K. (2016). Visualizing tumor evolution with the fishplot package for R. BMC Genomics *17*, 880.

Miller, C.A., White, B.S., Dees, N.D., Griffith, M., Welch, J.S., Griffith, O.L., Vij, R., Tomasson, M.H., Graubert, T.A., Walter, M.J.*, et al.* (2014). SciClone: inferring clonal architecture and tracking the spatial and temporal patterns of tumor evolution. PLoS Comput Biol *10*, e1003665.

Mkrtichyan, M., Najjar, Y.G., Raulfs, E.C., Abdalla, M.Y., Samara, R., Rotem-Yehudar, R., Cook, L., and Khleif, S.N. (2011). Anti-PD-1 synergizes with cyclophosphamide to induce potent anti-tumor vaccine effects through novel mechanisms. Eur J Immunol *41*, 2977-2986.

Niknafs, N., Kim, D., Kim, R., Diekhans, M., Ryan, M., Stenson, P.D., Cooper, D.N., and Karchin, R. (2013). MuPIT interactive: webserver for mapping variant positions to annotated, interactive 3D structures. Hum Genet *132*, 1235-1243.

Olsson, A., Venkatasubramanian, M., Chaudhri, V.K., Aronow, B.J., Salomonis, N., Singh, H., and Grimes, H.L. (2016). Single-cell analysis of mixed-lineage states leading to a binary cell fate choice. Nature *537*, 698-702.

Pei, M., Niu, J., Li, C., Cao, F., and Quan, S. (2016). Identification and expression analysis of genes related to calyx persistence in Korla fragrant pear. BMC Genomics *17*, 132.

Riaz, N., Havel, J.J., Makarov, V., Desrichard, A., Urba, W.J., Sims, J.S., Hodi, F.S., Martin-Algarra, S., Mandal, R., Sharfman, W.H.*, et al.* (2017). Tumor and Microenvironment Evolution during Immunotherapy with Nivolumab. Cell *171*, 934-949 e915.

Rosenblatt, J., Glotzbecker, B., Mills, H., Vasir, B., Tzachanis, D., Levine, J.D., Joyce, R.M., Wellenstein, K., Keefe, W., Schickler, M.*, et al.* (2011). PD-1 blockade by CT-011, anti-PD-1 antibody, enhances ex vivo T-cell responses to autologous dendritic cell/myeloma fusion vaccine. J Immunother *34*, 409-418.

Saada-Bouzid, E., Defaucheux, C., Karabajakian, A., Coloma, V.P., Servois, V., Paoletti, X., Even, C., Fayette, J., Guigay, J., Loirat, D.*, et al.* (2017). Hyperprogression during anti-PD-1/PD-L1 therapy in patients with recurrent and/or metastatic head and neck squamous cell carcinoma. Ann Oncol *28*, 1605-1611.

Subramanian, A., Tamayo, P., Mootha, V.K., Mukherjee, S., Ebert, B.L., Gillette, M.A., Paulovich, A., Pomeroy, S.L., Golub, T.R., Lander, E.S.*, et al.* (2005). Gene set enrichment analysis: a knowledge-based approach for interpreting genome-wide expression profiles. Proc Natl Acad Sci U S A *102*, 15545-15550.

Tappeiner, E., Finotello, F., Charoentong, P., Mayer, C., Rieder, D., and Trajanoski, Z. (2017). TIminer: NGS data mining pipeline for cancer immunology and immunotherapy. Bioinformatics *33*, 3140-3141.

Wang, K., Li, M., and Hakonarson, H. (2010). ANNOVAR: functional annotation of genetic variants from high-throughput sequencing data. Nucleic Acids Res *38*, e164.

Wang, X., Xiong, M., Lei, C., and Zhu, F. (2015). The developmental transcriptome of the synanthropic fly Chrysomya megacephala and insights into olfactory proteins. BMC Genomics *16*, 20.

Westin, J.R., Chu, F., Zhang, M., Fayad, L.E., Kwak, L.W., Fowler, N., Romaguera, J., Hagemeister, F., Fanale, M., Samaniego, F.*, et al.* (2014). Safety and activity of PD1 blockade

by pidilizumab in combination with rituximab in patients with relapsed follicular lymphoma: a single group, open-label, phase 2 trial. Lancet Oncol *15*, 69-77.

Xiong, D., Wang, Y., Kupert, E., Simpson, C., Pinney, S.M., Gaba, C.R., Mandal, D., Schwartz, A.G., Yang, P., de Andrade, M.*, et al.* (2015). A recurrent mutation in PARK2 is associated with familial lung cancer. Am J Hum Genet *96*, 301-308.